Available online at www.sciencedirect.com

ScienceDirect

Ceramics International 40 (2014) 1765–1769

CERAMICS INTERNATIONAL

www.elsevier.com/locate/ceramint

Large scale production of spherical WO_3 powder with ultrasonic spray pyrolysis assisted by sol–gel method for hydrogen detection

Taisheng Yang, Yue Zhang*, Chen Li

Key Laboratory of Aerospace Materials and Performance, School of Materials Science and Engineering, Beihang University, Beijing 100191, China

Received 13 June 2013; received in revised form 8 July 2013; accepted 15 July 2013
Available online 22 July 2013

Abstract

The spherical WO_3 powder was prepared by a facile ultrasonic spray pyrolysis process assisted by a sol–gel method. The thermal analysis of tungsten oxide precipitate indicated that there is 10% weight loss in the temperature range of 25–350 °C with two distinct steps, which correspond to the loss of the interlayer water molecules and the coordinated water molecules. The crystal structure and morphology have been investigated by X-ray diffraction (XRD) and scanning electron microscopy (SEM). The results indicate that the XRD peaks for the obtained sample can be indexed to the orthorhombic $WO_3 \cdot H_2O$ and triclinic WO_3 with the crystal water being eliminated after heat treatment. The particle size distribution was characterized by laser particle size analyzer and the result shows a double distribution; 50% of the total volume is composed of particles which are smaller than 0.74 μm. The d.c. electrical response to hydrogen of the spin-coating thick film sensor has been measured in the temperature range from 200 °C to 300 °C. The results indicate that the sensor performs as a n-type semiconductor, and it shows the maximum and minimum responses at 200 °C and 300 °C, respectively, with nearly linear dependence on the hydrogen gas concentration.

Keywords: Gas sensor; Sol–gel; Ultrasonic spray pyrolysis; Sphere powder

1. Introduction

The use of hydrogen as a clean energy source has been expanded into various fields such as fuel cell vehicles, rocket power and household fuel cells. However, hydrogen is colorless, odorless, explosive and extremely inflammable with a low explosive limit of 4% in air. Developing gas sensors that are able to detect H_2 in the ppm scale has attracted strong research interest [1]. Tungsten trioxide has been extensively investigated as a candidate of the chemical semiconductor based sensors in the past few decades. In more recent studies tungsten oxide nanostructures (i.e. nanowires [2,3], nanobelts [4,5] and nanorods [6,7]) were investigated as chemical sensing materials due to their high sensitivity and low working temperatures resulting from their high surface to volume ratios. A large number of techniques (e.g., sol–gel [8,9], electrochemical [10], hydro- or solvothermal [5,11], thermal evaporation [12], template methods [4]) had been employed to synthesize the nanostructured tungsten oxide powders and films.

In the present work, a facile route of the sol–gel assisting ultrasonic spray pyrolysis technique has been employed to synthesize the tungsten trioxide sphere powder with low energy comsumption and simple equipments. The hydrogen sensitivity at different operating temperatures has also been investigated and discussed.

2. Experimental details

2.1. Preparation of the precursor sol

Thirty grams of tungsten hexachloride (WCl_6, purity 99.5%, Huajing Powder Materials Science & Technological Co., Ltd. Changsha) was dissolved in 300 ml ethanol with continuous magnetic stirring under N_2 atmosphere. The solution was first transparent bright yellow, and then slowly turned to light blue before suddenly changing to dark blue. Excessive amount of

*Corresponding author. Tel./fax: +86 10 82316976.
E-mail address: zhangy@buaa.edu.cn (Y. Zhang).

0272-8842/$ - see front matter © 2013 Elsevier Ltd and Techna Group S.r.l. All rights reserved.
http://dx.doi.org/10.1016/j.ceramint.2013.07.076

deionized water was added into the solution after further magnetic stirring for about 30 min to obtain the tungsten hydroxide precipitate. The precipitate was washed several times with deionized water until the Cl^- ions were no longer detectible. The light yellow transparent peroxotungsten acid solution was obtained by mixing the precipitate with excessive amount of 30 mass% H_2O_2, and then the sol solution was diluted by deionized water for ultrasonic spray pyrolysis process.

2.2. Ultrasonic pray pyrolysis process

The schematic diagram of the ultrasonic spray pyrolysis process is shown in Fig. 1. The obtained precursor sol was ultrasonically atomized and carried by air, followed by heating and crystallization at 650 °C. The tungsten oxide sphere powder was collected after the exhaust was washed with deionized water and dried at 60 °C.

2.3. Powder characterization

TG–DSC measurement was carried out on a Perkin Elmer Pyris 1 TGA Analyzer (TG/DSC) coupled with A NETZSCH STA 449 F3 Jupiter thermal analyzer at a heating rate of 10 °C/min in dry air. An X-ray diffractometer (XRD, type Hytachi, Japan, with Cu Kα radiation $\lambda = 0.15406$ nm) was used to identify the crystal structures of the obtained samples. The microstructures of the samples were investigated using the scanning electron microscopy (SEM, CamScan Apllo300) and the transmission electron microscopy (TEM, JEOL JEM-2100). The particle size distribution was characterized by the laser particle size analyzer (Honeywell Microtrac X100).

2.4. Thick film sensitivity test

Pt wire contacts were attached to the two ends of the thin films with moderate-temperature silver paste before annealing at 550 °C for 1 h for electrical measurements. The conductance of the thin films was obtained by measuring the current through the film at a constant voltage of 5 V. The samples under test were placed in a sealed alumina tube in a Faraday cage inside an electrical furnace and exposed to different concentrations of hydrogen vapor through the gas-mixer controlled by mass flow meters after mixed. All gases were injected in parallel to the films with a flow rate of 600 ml/min. Gas sensitive properties of the films were studied in the temperature range of 200–300 °C, and the current values were read by a multimeter (Keithley 2601).

Sensor response, R_s, is defined as $(I_{gas} - I_0)/I_0$, where I_0 is the base resistance of the film measured in dry synthetic air, and I_{gas} is the current measured at the end of the H-loading process.

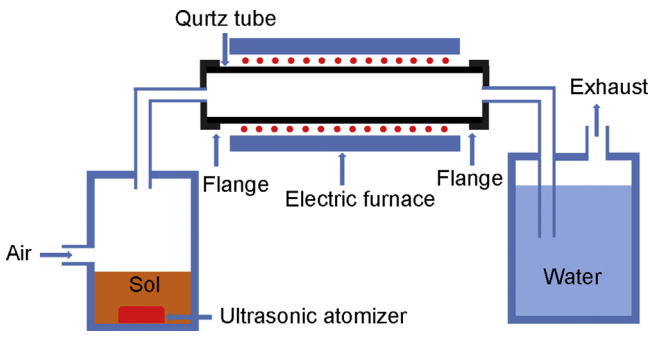

Fig. 1. Schematic diagram of the spray pyrolysis process.

3. Results and discussion

In order to evaluate the tungsten oxide content at the precipitate and the crystallization temperature during the spray pyrolysis process, TG/DSC experiments were performed. In Fig. 2, TG shows that there is about 10% weight loss as the temperature reaches 350 °C with two distinct steps. The result is consistent with the work of Li et al. [13] who studied the dehydration of $WO_3 \cdot H_2O$ and concluded that the first step near 70 °C was due to the loss of interlayer water molecules and the second step at higher temperature was due to the loss of coordinated water molecules. The endothermic peaks at about 100 °C and 270 °C in the DSC spectrum correspond to the loss of water molecules [14]. Additionally, amorphous tungsten gel transformed into crystalline WO_3 at about 420 °C, where a very sharp peak can be seen and this is consistent with the results reported in Ref. [15,16].

Fig. 3 presents the SEM image (a) and the XRD patterns (b) of the obtained powder. The spherical particles (Fig. 3a) have an overall size with diameters ranging from 200 to 800 nm. The XRD peaks can be indexed to the orthorhombic $WO_3 \cdot H_2O$ (JPCDS card no. 43-0679) and triclinic WO_3 (JPCDS card no. 20-1323) phases as shown in Fig. 3b. The formation of $WO_3 \cdot H_2O$ phase should be strongly related to the high temperature moisture during the spray pyrolysis process.

The spherical particles were further studied by using JEM-2100 to examine the microstructure. The TEM images are shown in Fig. 4. The particle shows a perfect spherical structure, and the HRTEM image reveals that the particle has a crystal form while its surface is constructed by much smaller

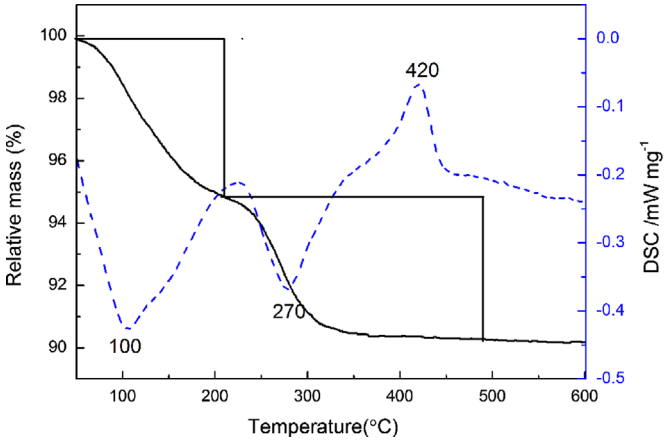

Fig. 2. TG–DSC curves for tungsten oxide precipitate from room temperature to 600 °C in dry air with a heating rate of 10 °C/min.

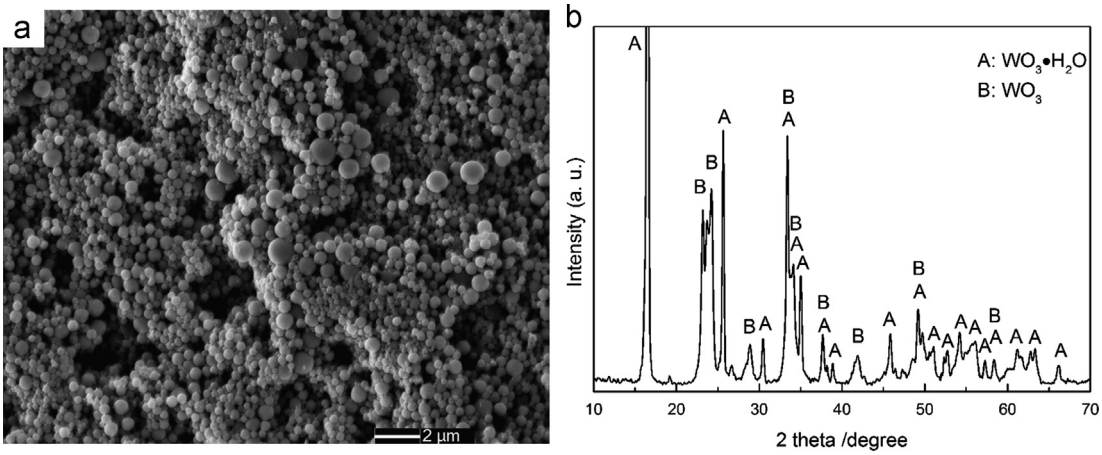

Fig. 3. XRD patterns (a) and SEM image (b) of the synthesized tungsten hydroxide/oxide sphere powder.

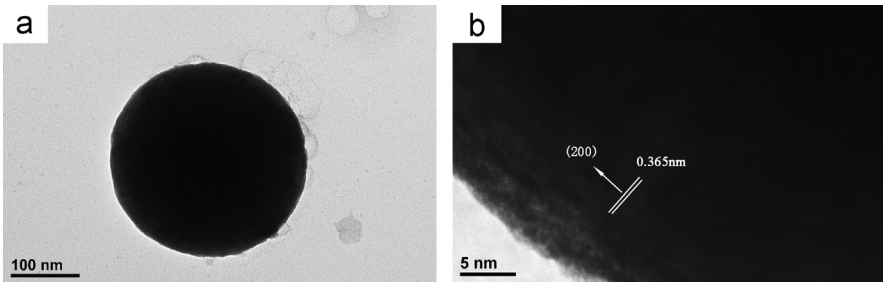

Fig. 4. TEM and HRTEM images of the obtained powder.

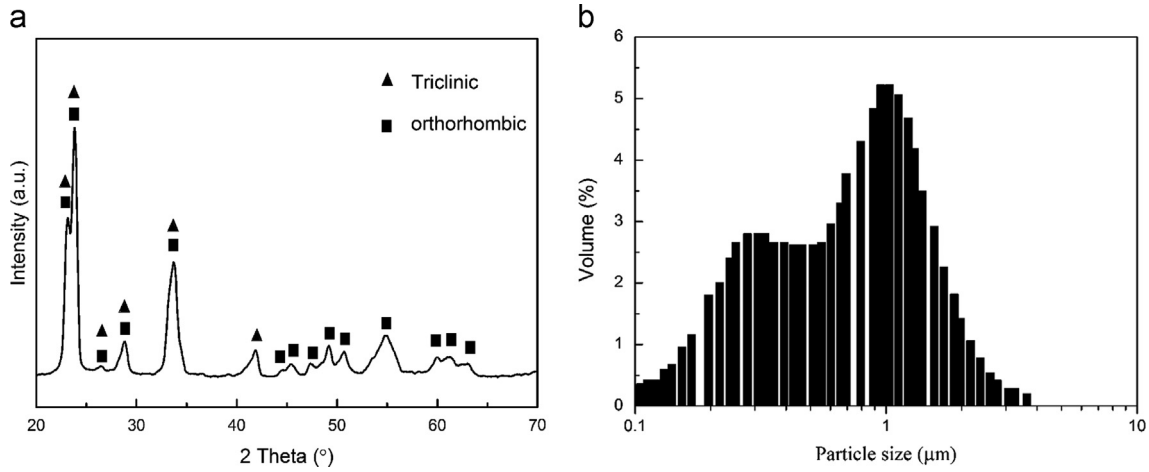

Fig. 5. XRD patterns (a) and the laser particle of the obtained powder (b) after being heat treated at 300 °C for 6 h.

crystal particles. We propose that there are two different regions in the structure, the inner one is composed of triclinic tungsten oxide while the outer one is composed of tungsten hydroxide, which are formed during different periods; the triclinic tungsten oxide is formed in the pyrolysis crystallization process while the tungsten hydroxide is formed due to the hot moisture.

The obtained powder was heat treated at 300 °C for 6 h to eliminate the chemical structure water molecules since the tungsten hydroxide shows considerably high proton conductivity [13,17,18]. The XRD peaks shown in Fig. 5a can be indexed to the triclinic (JPCDS card no. 32-1395) and orthorhombic (JPCDS card no. 20-1324) tungsten oxide, indicating that the orthorhombic $WO_3 \cdot H_2O$ has been completely eliminated. Furthermore, the particle size distribution of the obtained powder is presented in Fig. 5b, and the result indicates that the particle sizes range from 0.1 μm to 4 μm with a double distribution model. The particles with diameters smaller than 0.74 μm occupy about volume 50% of the powder.

The dynamic responses towards H_2 gas of various concentrations at 250 °C has been investigated and shown in Fig. 6. The conductance increases upon exposure to H_2 vapor indicating the

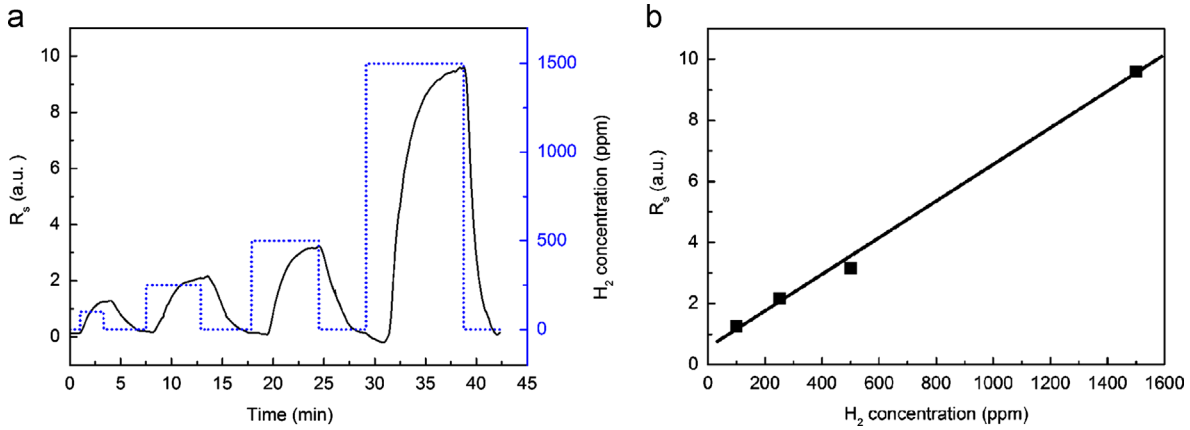

Fig. 6. Responses of the tungsten oxide thick films with different hydrogen concentrations at 250 °C (a) and its linear plot (b).

n-type semiconductor behaviors and our measurement showing good reproducibility. It is obvious that the higher H_2 concentration during exposure, the higher response is generated (Fig. 6a). The response exhibits a nearly linear relation with the H_2 concentration (ppm) as shown in Fig. 6b (the linear regression was performed with four replicates).

Fig. 7 represents the dynamic responses of the thick films exposed to 250 ppm hydrogen vapor at 200 °C, 250 °C and 300 °C. It is clear that both the response amplitude and the response time decrease with increasing operation temperature. This can be attributed to the surface reaction rates of both oxygen and hydrogen species. The equation describing the oxygen chemisorption can be written as [19,20]:

$$\frac{1}{2}O_2^{gas} + \alpha e^- + S \rightleftharpoons O_S^{-\alpha} \quad (1)$$

where S stand for an unoccupied chemisorption site; α can take 1/2, 1 and 2, which represent the O_2^-, O^- and O^{2-} species, respectively; $O_S^{-\alpha}$represents the chemisorbed oxygen at site S.

The reaction of a reducing gas A (here hydrogen) with ionosorbed oxygen species can be expressed by the following equation [19,20]:

$$A^{gas} + O_S^{-\alpha} \rightarrow AO^{gas} + \alpha e^- + S \quad (2)$$

where AO^{gas} is the reaction product.

It is shown by using TPD, FT-IR and ESR that the interaction with atmospheric oxygen with SnO_2 surface [21–23] leads to the ionic sorption in molecular (O_2^-) and atomic (O^-) forms at temperatures between 100 and 500 °C. Consequently, the atomic form dominates, leading to a pronounced increase of surface trap concentration above 200 °C. These result in the decline in the total number of free carriers [24]. The decrease of the response time at higher temperatures might be due to the faster rates of adsorption and desorption of H_2 molecules at the surface of WO_3 sensing film.

4. Conclusion

The tungsten oxide sphere powder has been prepared with ultrasonic spray pyrolysis assisted by sol–gel method. The obtained powder shows the orthorhombic and triclinic WO_3 structures after heat treatment at 300 °C for 6 h. The particle size distribution shows a double distribution model, the particles with diameters smaller than 0.74 μm consist of about volume 50% of the powder. The spherical powder thick film sensor shows a good, reversible and nearly linear response on the hydrogen concentrations at different temperatures. The response mechanism is related to the adsorption concentration of the ions and the reaction rates.

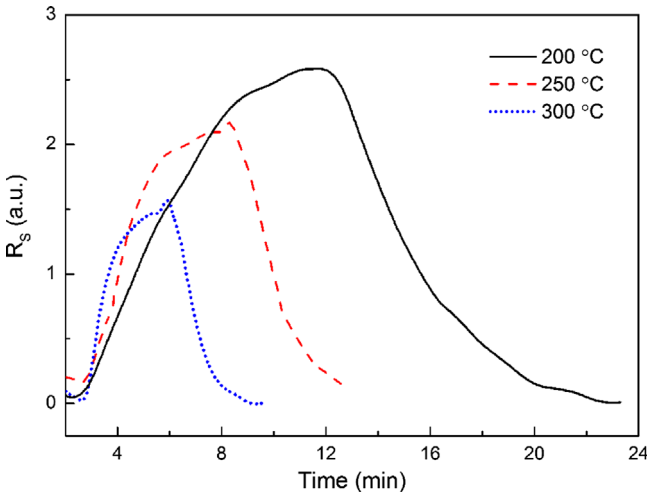

Fig. 7. Responses of the tungsten oxide thick films with 250 ppm hydrogen at different operation temperatures.

References

[1] V. Aroutiounian, Metal oxide hydrogen, oxygen, and carbon monoxide sensors for hydrogen setups and cells, International Journal of Hydrogen Energy 32 (9) (2007) 1145–1158.
[2] D. Meng, N.M. Shaalan, T. Yamazaki, T. Kikuta, Preparation of tungsten oxide nanowires and their application to NO_2 sensing, Sensors and Actuators B: Chemical 169 (0) (2012) 113–120.
[3] J. Choi, J. Kim, Highly sensitive hydrogen sensor based on suspended, functionalized single tungsten nanowire bridge, Sensors and Actuators B: Chemical 136 (1) (2009) 92–98.
[4] R. Artzi-Gerlitz, K.D. Benkstein, D.L. Lahr, J.L. Hertz, C. B. Montgomery, J.E. Bonevich, S. Semancik, M.J. Tarlov, Fabrication and gas sensing performance of parallel assemblies of metal oxide

nanotubes supported by porous aluminum oxide membranes, Sensors and Actuators B: Chemical 136 (1) (2009) 257–264.
[5] Y. Qin, M. Hu, J. Zhang, Microstructure characterization and NO_2-sensing properties of tungsten oxide nanostructures, Sensors and Actuators B: Chemical 150 (1) (2010) 339–345.
[6] A. Ponzoni, V. Russo, A. Bailini, C.S. Casari, M. Ferroni, A. Li Bassi, A. Migliori, V. Morandi, L. Ortolani, G. Sberveglieri, C.E. Bottani, Structural and gas-sensing characterization of tungsten oxide nanorods and nanoparticles, Sensors and Actuators B: Chemical 153 (2) (2011) 340–346.
[7] Y.S. Kim, Thermal treatment effects on the material and gas-sensing properties of room-temperature tungsten oxide nanorod sensors, Sensors and Actuators B: Chemical 137 (1) (2009) 297–304.
[8] J. Shieh, H.M. Feng, M.H. Hon, H.Y. Juang, WO_3 and W–Ti–O thin-film gas sensors prepared by sol–gel dip-coating, Sensors and Actuators B: Chemical 86 (1) (2002) 75–80.
[9] A.K. Srivastava, S.A. Agnihotry, M. Deepa, Sol–gel derived tungsten oxide films with pseudocubic triclinic nanorods and nanoparticles, Thin Solid Films 515 (4) (2006) 1419–1423.
[10] J. Kukkola, J. Mäklin, N. Halonen, T. Kyllönen, G. Tóth, M. Szabó, A. Shchukarev, J.-P. Mikkola, H. Jantunen, K. Kordás, Gas sensors based on anodic tungsten oxide, Sensors and Actuators B: Chemical 153 (2) (2011) 293–300.
[11] D. Ding, Y. Shen, Y. Ouyang, Z. Li, Hydrothermal deposition and photochromic performances of three kinds of hierarchical structure arrays of WO_3 thin films, Thin Solid Films 520 (24) (2012) 7164–7168.
[12] M. Ahsan, M.Z. Ahmad, T. Tesfamichael, J. Bell, W. Wlodarski, N. Motta, Low temperature response of nanostructured tungsten oxide thin films toward hydrogen and ethanol, Sensors and Actuators B: Chemical 173 (0) (2012) 789–796.
[13] Y.M. Li, M. Hibino, M. Miyayania, T. Kudo, Proton conductivity of tungsten trioxide hydrates at intermediate temperature, Solid State Ionics 134 (3–4) (2000) 271–279.
[14] M. Deepa, T.K. Saxena, D.P. Singh, K.N. Sood, S.A. Agnihotry, Spin coated versus dip coated electrochromic tungsten oxide films: structure, morphology, optical and electrochemical properties, Electrochimica Acta 51 (10) (2006) 1974–1989.
[15] R. Solarska, B. Alexander, J. Augustynski, Electrochromic and structural characteristics of mesoporous WO_3 films prepared by a sol–gel method, Journal of Solid State Electrochemistry 8 (10) (2004) 748–756.
[16] W. Li, J. Li, X. Wang, J. Ma, Q. Chen, Photoelectrochemical and physical properties of WO_3 films obtained by the polymeric precursor method, International Journal of Hydrogen Energy 35 (24) (2010) 13137–13145.
[17] P. Barboux, R. Morineau, J. Livage, Protonic conductivity in hydrates, Solid State Ionics 27 (4) (1988) 221–225.
[18] B. Mecheri, A. D′Epifanio, M.L. Di Vona, E. Traversa, S. Licoccia, M. Miyayama, Proton Conducting Electrolyte Membranes based on Tungsten Oxide and Sulfonated Polyether Ether Ketone Hybrid Composites, MRS Online Proceedings Library, 2005.
[19] N. Barsan, U. Weimar, Conduction model of metal oxide gas sensors, Journal of Electroceramics 7 (3) (2001) 143–167.
[20] S. Zhang, C. Xie, H. Li, Z. Bai, X. Xia, D. Zeng, A reaction model of metal oxide gas sensors and a recognition method by pattern matching, Sensors and Actuators B: Chemical 135 (2) (2009) 552–559.
[21] S. Lenaerts, J. Roggen, G. Maes, FT-IR characterization of tin dioxide gas sensor materials under working conditions, Spectrochimica Acta Part A: Molecular and Biomolecular Spectroscopy 51 (5) (1995) 883–894.
[22] N. Yamazoe, J. Fuchigami, M. Kishikawa, T. Seiyama, Interactions of tin oxide surface with O_2, H_2O and H_2, Surface Science 86 (0) (1979) 335–344.
[23] S.-C. Chang, Oxygen chemisorption on tin oxide: correlation between electrical conductivity and EPR measurements, Journal of Vacuum Science and Technology 17 (1) (1980) 366–369.
[24] A. Oprea, E. Moretton, N. Barsan, W.J. Becker, J. Wollenstein, U. Weimar, Conduction model of SnO_2 thin films based on conductance and Hall effect measurements, Journal of Applied Physics 100 (3) (2006) 033710–033716.